Proceedings of ASME Turbo Expo 2024
Turbomachinery Technical Conference and Exposition
GT2024
June 24-28, 2024, London, United Kingdom

GT2024-128871

AN EXPERIMENTAL CASE STUDY IN COMBINING TOPOLOGY OPTIMIZATION AND ADDITIVE MANUFACTURING TECHNIQUES TO GENERATE NOVEL AND HIGH-PERFORMANCE COMPACT HEAT EXCHANGER DESIGNS

Thomas W. Rees[1], Abdullah Azam[2], Nicola Casari[1], Polly Banks[2], Lukas Jiranek[2], Stefano Furino[1], Arun Muley[3]

[1]ToffeeX, London, United Kingdom
[2]Boeing, Sheffield, United Kingdom
[3]Boeing, Huntington Beach, USA

NOMENCLATURE

AM	Additive Manufacturing
DfAM	Design for Additive Manufacturing
TO	Topology Optimization
RANS	Reynolds Averaged Navier Stokes
HX	Heat Exchanger
ROM	Reduced-Order Model
CHT	Conjugate Heat Transfer
HTC	Heat Transfer Coefficient
Re	Reynolds number
Nu	Nusselt number
α	Secondary design variable
γ	Design variable
Γ	Design domain boundary
Ω	Design domain
ν	Kinematic viscosity
ρ	Density
ω	Objective weighting constant
R_i	Optimization constraint
F	Objective function
$\boldsymbol{u}$	Velocity
P_0	Total pressure
E	(Thermal) Energy
$\hat{\boldsymbol{n}}$	Normal unit vector
$\boldsymbol{X}$	Generic dependent design variable
p	Pressure
D	Diffusivity coefficient
$Q_{cond/conv}$	Conductive/convective heat transfer
S	Heat transfer surface area
$R_{cond/conv}$	Conductive/convective resistance
k	Thermal conductivity
h	Heat transfer coefficient
l	Heat transfer length scale

ABSTRACT

The recent industrialization of additive manufacturing processes has led to research interest in alternative, more complex two-fluid heat exchanger designs, such as those constructed from repeating triply periodic unit cell geometries like gyroids, Schwarz minimal surfaces or other complex geometries. These types of designs are particularly convenient because their performance can be scaled up or down by including more or fewer periodic unit cells in the final heat exchanger lattice. Despite their complexity, repeating periodic unit cell-based heat exchanger designs have not been shown to have performance advantages over more traditional designs and therefore have yet to find widespread industrial application. This failure is partially due to the fact that the periodic unit cells used to build these heat exchangers are not optimized for thermo-fluid efficiency, as well as the fact that accurate simulation of a heat exchanger containing thousands of complex unit cells is extremely challenging, making the design of the overall heat exchanger difficult.

This paper presents the results of a project to develop a heat exchanger design method which can overcome these deficiencies. In particular, we design, build, and test a crossflow two-fluid heat exchanger based on a periodic unit cell designed using a proprietary topology optimization algorithm. The heat exchanger is manufactured using additive manufacturing. Analysis of the unit cell design showed that it generated secondary flows to increase the effectiveness of the heat transfer while also minimizing unnecessary loss-generating flow structures. The performance of the entire heat exchanger was simulated computationally using RANS-based CFD simulations on a single unit cell. The results of this simulation were used to build a reduced-order model to predict the heat transfer and pressure drop across the entire heat exchanger at two representative operating conditions.

After numerical simulation, the final design was manufactured from stainless steel using a Renishaw 500Q machine and its performance was measured experimentally. The experimental results are favorably compared against the numerical predictions to validate both the CFD simulations on the periodic unit cell as well as the reduced order model of the entire heat exchanger. This indicates that the topology optimization design process can be confidently applied to design scalable heat exchangers.

Keywords: heat exchanger, periodic unit cell, topology optimization, additive manufacturing

1. INTRODUCTION

The drive towards sustainable aviation is linked to overcoming the thermal management challenges faced by the aviation industry [1]. Aerospace thermal management is becoming increasingly challenging due to the modernization of aircraft through, for example, electrification and the use of composites. The electrification of aircrafts manifests in challenges associated with low grade heat management, while the use of composites results in inefficient heat loss compared to metals. Modern aircraft are expected to deal with much larger thermal dissipation in the range of megawatts compared to kilowatts [2].

Two fluid heat exchangers are a widely used and necessary component of many different industrial systems where efficient heat transfer is necessary. In the context of commercial airliners, heat exchangers are used in environmental control systems, power electronics cooling, engine oil coolers, and hydraulic fluid heat exchangers [3].

Traditionally, two fluid heat exchanger designs for aerospace have used brazed plate-fin designs due to their high efficiency and compact nature [3]. However, as described above, in recent years aerospace thermal management has been faced with challenges due to electrification and hydrogen propulsion, long heat transport of heat due to composite structures (low thermal conductivity), low grade heat extraction and in some cases, the actual airframe cooling is required to improve its survivability [4]. Specifically, in commercial airlines technology, the thermal load management is becoming an ever-increasing challenge due to modern wing architectures, electrification at system level, and introduction of high bypass ratio engines [5] [6]. This has led to aerospace engineers to investigate alternative, more complex heat exchanger designs. These activities have primarily been driven by requirements for increased heat transfer efficiency, reduced weight, and size [7].

Additive Manufacturing (AM) has recently become a hot topic in aerospace due to the ability to rapidly prototype and manufacture complex shapes allowing high levels of design freedom. To take full advantage of the performance gains offered by the geometries which are manufacturable using additive techniques, design for additive manufacturing (DfAM) techniques are necessary [8]. Simply reproducing existing heat exchanger designs using AM is unlikely to offer the step change in performance necessary to justify development and certification of these new geometries.

Engineers have generally tried to address this challenge in two ways: by improving existing design with features that can only be made using additive methods [8], which only offers incremental design improvements. More radical heat exchanger re-designs have in general focused on creating periodic unit cell lattices from libraries of triply periodic structures such as gyroids or Schwarz bodies [9].

Reduced lead time is at present the main driver for using AM in aerospace [10]. Despite the advantages offered offered by additive, one of the easiest lead-time reduction methods is managing the certification burden by re-using existing designed elements to realize a separate certified part. The highly regulated nature of aerospace engineering means that component certification requirements are a very important consideration during the design process.

One solution to enable an easier or faster certification process across aircraft platforms is to design components using a modular approach. In this way, when a single module of the component has been certified, the certification process of a multi-module component is made easier. This requires the repeating units to be scaled up or down to match the required performance. This scaling relationship is not simple and simulations of larger sets of unit cells is impractical. Therefore, validation of such models and approaches is crucial for building confidence in such methodologies.

The scope of this paper is to develop a new design technique which can leverage the advantages of additive manufacturing by generating high-performance designs while also allowing lead-time reduction by taking advantage of unit-cell based designs to minimize possible certification burdens. Specifically, we propose a method of generating a lattice of repeating units which show very high thermos-fluid performance using fluid topology optimization. These units are proved to be manufacturable with existing additive techniques and the performance is proven to be predictable (to a first order, early-stage design level) by comparison to experimental tests.

2. TOPOLOGY OPTIMIZATION

Topology optimization (TO) is a mathematical optimization method which finds an optimal distribution of a scalar design/optimization variable γ in a domain Ω with boundaries Γ while simultaneously respecting a set of linear or nonlinear constraints $R_i = 0$, which are usually (but not always) chosen to represent a set of physical governing equations for the problem [11]. TO problems are solved iteratively as an adjoint-based optimization problem (either discrete or continuous), with γ being updated with an optimization method such as gradient descent [12] or the method of moving asymptotes [13].

We note here that an 'optimal' solution found by a TO algorithm can only be a local optimum, rather than a global optimum. This is because adjoint methods are based on Lagrange multiplier theory, which is a necessary, but not sufficient condition. Therefore, it is important that *a posteriori* analysis of each TO result be done to evaluate its performance against other

TO results. It is during this evaluation that engineers must make their best judgement on the component design which best suits their needs.,

In industrial applications, topology optimization is primarily used as a structural design tool for applications such as lightweighting of structural members such as brackets, struts, or cantilevers [14]. Recent research has explored the idea of using TO for more complicated physical problems such as fluid dynamics [15] or electromagnetics [16]. These are far more challenging problems due to the nonlinearity of their governing equations (Navier-Stokes equations for fluid dynamics) or the number of state variables and governing equations (Maxwell's equations for electromagnetics). Topology optimization has also been applied to multi-physics problems where multiple governing equation systems are coupled to represent far more complicated physical problems. An example is thermo-fluid topology optimization, where the Navier Stokes equations are coupled to a thermal energy conservation equation [12].

In the scientific literature, TO techniques have also been developed to optimize two fluid heat exchanger designs [17] [18]. The primary challenge in developing a TO problem statement for two fluid heat exchangers is the requirement to impose an extra constraint on the optimization problem (in addition to the governing equations) to ensure that the two fluids involved in the problem statement stay separate and do not mix.

Both Høghøj et al. [17] and Kobayashi et al. [18] achieved this by using a single design variable $\gamma \in [0,1]$ for the two fluid problem, from whose value the secondary design variables α_1 and α_2 can be calculated. These latter two values represent a Brinkmann-style impermeability which is used to represent the presence of a solid material in the optimization domain [15].

In summary, the objective function for the two fluid heat transfer TO problem can be stated as:

$$\min_{\gamma} F(\boldsymbol{X},\gamma) = \omega_1 \int_{\Gamma} P_{01}\boldsymbol{u_1}\cdot\hat{\boldsymbol{n}}d\Gamma + \omega_2 \int_{\Gamma} P_{02}\boldsymbol{u_2}\cdot\hat{\boldsymbol{n}}d\Gamma + \omega_3 \int_{\Gamma} E\boldsymbol{u}\cdot\hat{\boldsymbol{n}}d\Gamma \quad (1)$$

This objective function represents a weighted sum of individual terms representing 1) total pressure losses in the first fluid, 2) total pressure losses in the second fluid and 3) heat transfer to/from the first fluid. Assuming adiabatic walls, the last term in the objective function represents the heat duty of the entire heat exchanger. This objective function is minimized subject to the following constraints:

$$R_{p_1} = \nabla\cdot\boldsymbol{u_1} = 0 \quad (2)$$

$$R_{p_2} = \nabla\cdot\boldsymbol{u_2} = 0 \quad (3)$$

$$R_{\boldsymbol{u_1}} = \boldsymbol{u_1}\cdot\nabla\boldsymbol{u_1} + \frac{\nabla p_1}{\rho_1} - \nu_1\nabla^2\boldsymbol{u_1} + \alpha_1(\gamma)\boldsymbol{u_1} = 0 \quad (4)$$

$$R_{\boldsymbol{u_2}} = \boldsymbol{u_2}\cdot\nabla\boldsymbol{u_2} + \frac{\nabla p_2}{\rho_2} - \nu_2\nabla^2\boldsymbol{u_2} + \alpha_2(\gamma)\boldsymbol{u_2} = 0 \quad (5)$$

$$R_{\boldsymbol{E}} = (\boldsymbol{u_1}+\boldsymbol{u_2})\cdot\boldsymbol{\nabla}E - \nabla\cdot(D\nabla E) = 0 \quad (6)$$

The constraints correspond to a modified system of Navier-Stokes equations for each of the two fluids, written for an incompressible, steady-state problem. The additional terms in the momentum equations are commonly referred to as Brinkmann terms. They represent a momentum sink due to the solid material being formed as the optimization proceeds. These block the flow of the fluid through these regions. This term ensures that the fluid velocity is non-zero only where the solid is not present – therefore in the pure fluid areas. Because of this, the unified form of the energy equation (6) represents a pure diffusion equation in the solid (because in these regions $\boldsymbol{u_1} = \boldsymbol{u_2} = \boldsymbol{0}$) and an advection-diffusion equation in each of the fluid regions.

The constraints must also include an appropriate set of boundary conditions for the governing equations. For all the non-periodic TO simulation results presented in the present work, the following set of boundary conditions is used:

- Inlet: Dirichlet condition on velocity and temperature, Neumann on pressure
- Outlet: Neumann condition on temperature and velocity, Dirichlet on pressure
- Walls: Dirichlet on velocity (no-slip) and Neumann for pressure and temperature (adiabatic)
- Symmetry planes: symmetry condition

In the case of the periodic boundary conditions used to generate the periodic unit cells described in the latter sections of this paper, a set of triply periodic boundary conditions are used. Periodicity in the streamwise direction is achieved by applying a constant pressure gradient source term to the momentum equations (4) and (5) which drives the flow. Periodicity in the temperature system is much more challenging, but is achieved by careful normalization of the temperature field at the inlet and outlet of the periodic unit cell during the solution of the equations.

2.1 TOFFEEX PHYSICS DRIVEN GENERATIVE DESIGN TOOL

The two fluid heat exchanger designs presented in this paper were generated using the ToffeeX physics-driven design computer aided engineering software tool. Based primarily on TO methods such as those described in the previous section, ToffeeX uses a finite volume method Reynolds-averaged Navier Stokes (RANS) solver to solve the governing equations based on user defined boundary conditions. The solid field is represented in the fluid TO problem with a Brinkmann impermeability term, however both the optimization solver as well as the precise TO model are proprietary.

In addition to providing the boundary conditions and the design domain for the topology optimization problem, ToffeeX users must provide information about the fluid(s) and solid material(s) to be used in the TO simulation. Users can also specify global and local geometry constraints and physics effects based on the specific requirements of the design (see Section 3).

2.2 POWDER BED FUSION ADDITIVE MANUFACTURING

Powder Bed Fusion (PBF) is a method of AM that has advanced significantly in industry following extensive research and development and is a mature process with widespread use. PBF follows the process of metallic powder being transferred from a powder dispensing location to the machine's build platform, and a laser or electron beam melting the powder to fuse the material together. The powder is distributed from one side of the build platform to the other, and the build platform lowers after a layer is deposited, so that the material can be built up and fused together, to produce the final geometry. To distribute the powder, the material supply in the powder hopper or reservoir ascends and a blade or roller is used to spread it across the build platform. Excess powder is used during the layering process to ensure there is sufficient coverage, and any further excess after the layer is complete may be deposited at the other end of the build platform. It is common for unfused powder to be present on the final build, however this is removed during post processing steps.

3. DESIGN PROCESS AND RESULTS

Physics-driven generative design engineering tools offer engineers the ability to rapidly generate designs and iterate through the design process. In this section we present a subset of design iterations generated with ToffeeX as part of this work to illustrate the rapid iteration process. During this iterative process, the design and simulations problems submitted to the ToffeeX software were changed based on several considerations, not only from the perspective of the heat exchanger's performance but also based on the requirements for manufacturing and testing, as well as simply the limitations of the ToffeeX tool and technology, in such a way as to maximize the effectiveness of the tool.

Many different approaches for the design of an HX are possible, spanning from full scale HX to a very small "unit cell" which can be repeated to form a lattice.

- **2D type optimization**: this type of optimization can be described as "topology optimized plate-fin". The available space is subdivided in parallel layers and each of them is topologically optimized. The resulting structure is typically constrained to be an extruded 2D design, and therefore this approach can be used both for additive manufacturing and more traditional techniques, as each of the layer can be machined or chemically etched and then bonded or brazed to build a plate-fin-style heat exchanger. A simplified example of the resulting structure is reported in Fig**.** 1

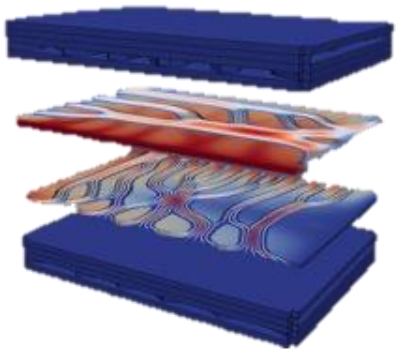

Figure 1: Result of a 2D type optimization. The geometry is extruded in the 3rd direction to form a plate-type HX

- **3D monolithic optimization:** this approach is limited to AM methods. For this case, a conventional set of 3D equations is solved. his approach grants full 3D freedom in the geometric complexity. However, the mesh resolution necessary for the simulation and topology optimization is usually far too large to yield a computationally feasible topology optimization problem. An example of the resulting geometry is reported in Fig 2. Note the complexity is far too low to provide acceptable heat transfer over the entire heat exchanger.

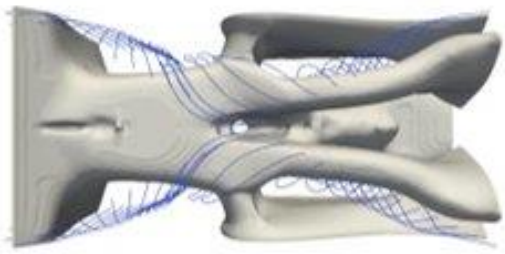

Figure 2: Result of a quasi-periodic type optimization.

- **Periodic 3D optimization:** this approach is limited to AM methods. For this case, a set of 3D equations including a constant periodic pressure gradient is solved. This approach grants full 3D freedom in the geometric complexity. A typical example of unit cell and array of unit cells is reported in Fig. 3. This approach has been developed specifically for this project and represents a novelty in the literature to the authors' knowledge.

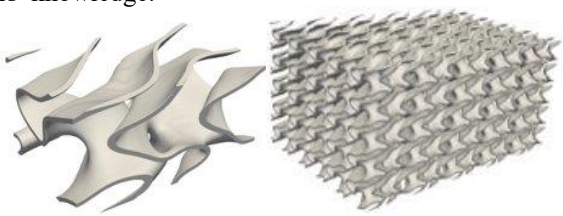

Figure 3: Result of a periodic type optimization. Unit cell on the left-hand side and array of unit cells to form an HX

The preferred method is left to the user, but the approach used in this work is to let the TO design a single unit cell, in a triply periodic 3D optimization. The actual design is performed by selecting the dimension of the unit cell based on the preferred parameter (e.g. Reynolds number) and supplying to ToffeeX a design domain equal to the volume of that unit cell. This option is preferred in this work, mainly for computational costs considerations and for the easier rate of convergence for such a complex problem. Indeed, the direct optimization of the entire HX, although possible, would reflect in an extremely large computational costs, and the proper selection of pressure drop vs heat transfer objective would be extremely time consuming as a few iterations of the design process are needed.

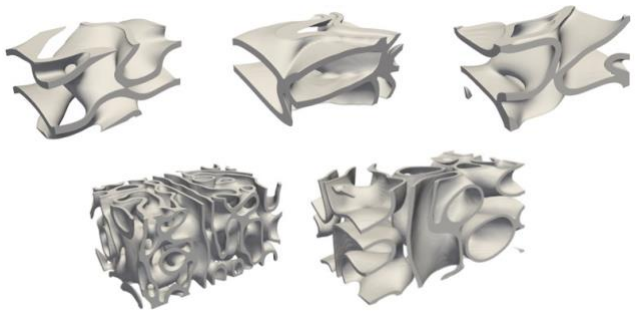

Figure 4: Candidate unit cell designs obtained by ToffeeX

3.1 PERIODIC UNIT CELL HEAT EXCHANGER

Several different designs were obtained, based on the relative importance given to heat transfer or pressure loss terms in the objective function. Some of the designs are reported in Figure 4. It is stressed here that each of the designs requires less of 1 hour to be generated, therefore it is possible to explore a very large solution domain before choosing the ideal shape.

Among the different designs obtained, the unit cell reported in Figure 5 was chosen as the candidate to continue the study with. This unit cell is composed of an airfoil-like obstacle in which is wetted outside from the hot fluid and inside it the fresh air is flowing. The membrane is 0.28 mm thick, and overhanging areas remain minimal. In fact, this was the primary reason for choosing this design over the other candidate designs (despite a slightly lower performance prediction).

In order to create the structure of the entire heat the unit cell must be joined, creating a lattice of 20x20x20 units. A portion of the lattice is shown in Figure 6.

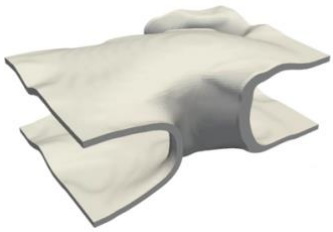

Figure 5: Unit Cell used for the HX design

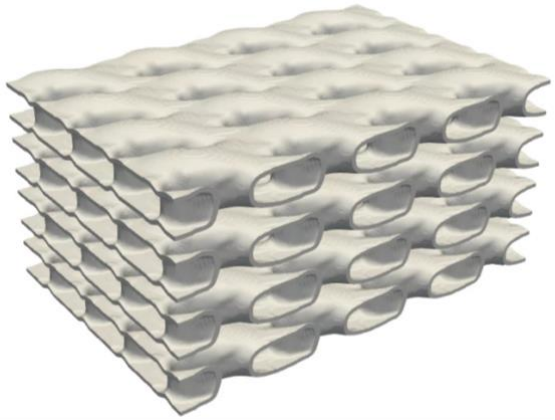

Figure 6: Lattice of unit cells corresponding to a portion of the HX

4. HEAT EXCHANGER PERFORMANCE PREDICTION

The periodic unit cell topology optimization process assumes the flow is periodic in terms of flow structures across each of the cells. This is of course only an approximation of reality. However, preliminary CFD simulations of arrays of the unit cell (Figure 7) suggests that the flow rate is approximately periodic after passing through the first cell in the array. As the HX is composed of a 20x20x20 array of cells, an assumption of periodicity throughout the heat exchanger is appropriate to a first order approximation.

With this key simplification of periodicity in velocity and pressure fields confirmed, it is necessary to decuce the temperature distribution inside the HX and thus its overall thermodynamic performance. To predict the overall performance of the HX, we develop a Reduced Order Model (ROM) from the flow conditions at the inlet of hot and cold side and the shape of the unit cell. This approach is general and can be applied to any periodic HX if the above-mentioned information is available. The ROM developed for this project is a thermal-analogy-based model which is built according to the following steps:

1. CFD analysis of hot and cold sides of the unit cell separately (i.e. no CHT);
2. Extraction of the relevant (non-dimensional) performance parameters ($Nu, \Delta p$) for each of the fluids, for some relevant flow rates and temperatures.
3. Exploit the values at 2 for building the thermal resistance model.
4. The thermal resistance model calculates the heat which is lost by the hot fluid in each unit cell (and gained by the cold one). This heat is subtracted (added) from the enthalpy of each fluid to assess the temperature variation across the unit cell.

Each of these steps is described in detail below. It should be remarked here that the analysis regards a single layer only. The 3rd direction is composed of identical layers stacked one upon the other and for that reason it is assumed the evolution of the temperature is uniform along such direction, making the problem effectively 2D.

4.1 CFD analysis of hot and cold side

The performance assessment requires the flow field to be known inside the unit cell, as the underlying assumption here is that all the unit cells have the same flow pattern. To calculate this, the flow through a series of 7 cells has been calculated. The 4th unit cell is the one chosen as being relevant for the performance evaluation, as the flow is sufficiently periodic, and the outlet condition does not affect the flow pattern. Four different conditions are investigated, corresponding to the maximum and minimum flow rates reported in the experiments (identified as LowRe and HighRe), each at a cold temperature and a hot temperature. The corresponding BC of Tab. 1 are imposed.

Tab. 1: Boundary conditions applied for the "single fluid" calculations.

	Inlet			Outlet	Walls
Pressure [bar_a]	Zero Gradient			1	Zero gradient
Velocity [m/s]		N2	Air	Zero Gradient	No-slip
	LowRe	0.68	0.6		
	HigRe	3.38	3		
Temp [K]	N2	Air		Zero Gradient	Convective HT
	393	303			

In order to reduce the complexity and set-up time of these simulations, they are performed in a weakly coupled-manner, without building a multi-region fluid-solid-fluid mesh and running a complete conjugate heat transfer simulation. Instead, the weak coupling is achieved using a convective heat transfer boundary condition from which the heat transfer coefficient on both the hot and cold sides of the walls can be calculated

At the walls, the temperature boundary condition is a Neumann condition, where the temperature gradient is calculated from is calculated from a thermal resistance model. This model considers the thickness of the solid layer/membrane separating the two fluids and the temperature of the second fluid, and the heat transfer coefficient of the second fluid. For these preliminary analyses the temperature of the second fluid has been assumed to be constant and equal to the inlet temperature while the heat transfer coefficient is calculated from a separate CFD calculation using an isothermal wall.

The simulation performed is a steady state compressible simulation, with SST k-ω turbulence modeling. The accurate representation of flow structures inside such a complex geometry is a very challenging task, and the turbulence model plays a very important role. A comparison with the $\gamma - Re_\Theta$ transitional model has been carried out. The difference in the flow pattern recorded is not very significant, and probably a higher fidelity turbulence modelling would be required for good accuracy (i.e. LES), which would be extremely computationally expensive.

This procedure is repeated for each of the fluids thought as being independent one another and only weakly coupled by the thermal boundary condition at the wall.

4.2 Performances of each of the fluids

The parameters to be used for the ROM are extracted from the CFD carried out as described in Section 4.1. The flow field of the N2 (hot fluid) in the maximum velocity case is reported in Fig. 7. The flow becomes periodic almost immediately, as the nitrogen flow around the second and third airfoil-like element is very similar. The parameters for the ROM are extracted around the central airfoil.

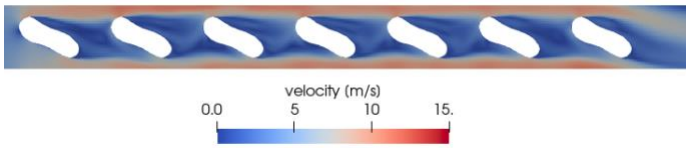

Figure 7. cross section of a 7-cells strip inside the hot side of the HX.

It is interesting to note that large flow separation occurs downstream the airfoil-shaped obstacle. This separation effectively promotes mixing and an accurate representation of it will influence performance. However, the separation physics will depend strongly on accurate turbulence modelling. As mentioned above, the high-fidelity turbulence modelling necessary to confirm this flow structure is beyond the scope of the work, and possible discrepancies of the heat transfer evaluation and pressure losses if compared to the experiments might be (in part) related to this misprediction.

The same approach has been applied to the air side of the HX to enable periodic flow to fully develop and to assess the performance of a unit cell. The airflow pattern for the high Reynolds case is reported in Figure 8.

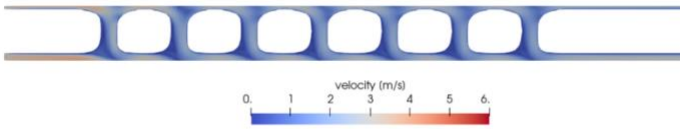

Figure 8. cross section of a 7-cells strip inside the air side of the HX.

Similar considerations with respect to the ones reported for the N2 side can be made on hair. The central cell is the one on which performances have been calculated. The relevant results for the N2 and air side are reported in Table. 2.

Table 2: Performances of the two fluids domains taken individually

	Air		N2	
	LowRe	HighRe	LowRe	HighRe
h [W/m2K]	35	75	36	87
dP [Pa]	0.17	2.5	1.0	15

4.3 Thermal Resistance model and Energy balance

The ROM calculates the heat transfer between the two fluids at the HX level by treating each individual unit cell from an electrical resistance analogy. The heat is transferred from the hot to the cold fluid by convection first between the hot fluid and the hot surface of the membrane, then by conduction within the membrane and lastly by convection between the cold side of the membrane and the membrane. Each of these mechanisms is modelled via an equivalent resistance.

$$\dot{Q}_{conv} = {\Delta T}/{R_{conv}} = {\Delta T}/{hS} \quad (7)$$

$$\dot{Q}_{cond} = {\Delta T}/{R_{cond}} = {\Delta T}/{\frac{k}{l}S} \quad (8)$$

All the parameters that appear in the former equations are retrievable from the CFD single-phase simulation as described in 3.1 and 3.2. The overall thermal resistance is then calculated as

$$R_{th} = \frac{1}{h_{cold}S} + \frac{1}{h_{hot}S} + \frac{l}{kS} \quad (9)$$

The former equations are used for assessing the heat flux through the membrane surface. To maintain the energy balance, this heat is subtracted by the enthalpy of the hot fluid and added to the enthalpy of the cold fluid. This approach enables to conserve the energy but also neglects the heat transfer to the surrounding environment. As the HX is not insulated in the experimental setup this remark is important as natural convection to the environment is not considered.

5. MANUFACTURING

The heat exchanger was manufactured from 316L stainless steel using a Renishaw 500Q machine, which has a build chamber size of 250 x 250 x 350 mm. The periodic unit cell STEP files generated by the topology optimization algorithm needed some initial cleaning and adjustment to tackle some overhanging regions which would have caused issues with the build process. An initial build was completed with standard Renishaw parameters for 316L. CT scans of this initial build showed the final structure having much thicker walls than those on the 3D model. A second build with build parameters adjusted slightly for thinner walls gave an average wall thickness of 330µm (still thicker than the 280 µm in the 3D model from the design software). No specific heat treatment was applied to the unit and simple pressurized air de-powdering was found to be sufficient. Two identical geometries were made using the same CAD file.

6. EXPERIMENTAL TESTING

The performance of the heat exchanger was validated by experiment. A schematic diagram of the experimental rig used is shown in Figure 9. The HX is equipped with two 1 m calming inlet and outlet channels to create fully developed flow in and out of the heat exchanger. The HX was secured with clamps between each of these two inlet and outlet channels and high temperature joint sealant applied. The hot air inlet channel was insulated. Both inlets had an inlet valve, a 120g/s flow meter, a type K thermocouple and a 3 bar (absolute) pressure gauge. The outlets had a type K thermocouple and a 3 bar (absolute) pressure gauge.

The pressure was measured by the pressure gauges, positioned 10cm from the inlets and outlets, in the center of the flow, and the static pressure ratios were determined (inlet/outlet). The thermocouples measuring the temperature difference across the unit were positioned in the channels 7.5cm from each inlet and outlet. The flow was regulated by a valve, and the outlets were fully open to have a continuous mass flow.

The last available calibration of the flow meters was used. The thermocouple has a device error of ±1.5°C and a tolerance of ±5°C. This is generally very high for thermocouples, but was a result of the last available calibration available for the set of thermocouples used. The pressure gauge has a device error of ±0.1%fs and a tolerance of ±0.2barg. The flow meter has a device error of ±1%.

The test set-up allowed for both the pressure ratios and temperature differences to be completed in a combined test. These quantities were determined for different mass flows, and are shown in Table 3. Note that the heat transfer values presented here are averages between the measured heat transfer on the hot and cold sides of the heat exchanger. Independently measured values of heat transfer vary by 10-12% per side (depending on the high or low temperature cases. This indicates significant losses to the environment (discussed below). Although an extensive experimental campaign was carried out, only the results to be compared with the high Re and low Re cases are reported here.

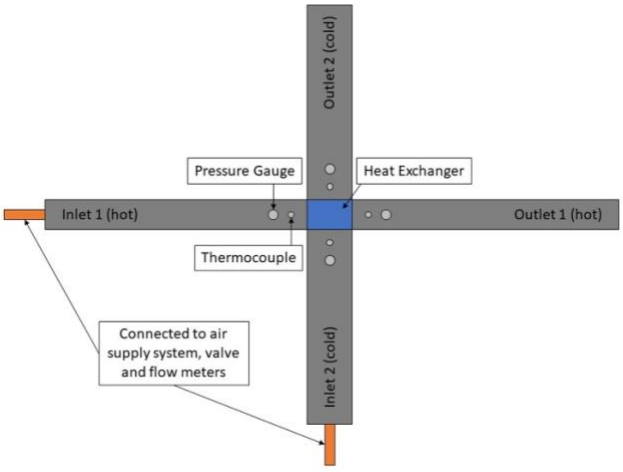

Figure 9: Experimental setup schematic for HX testing

To better show the behavior of the HX in different operating conditions, the normalized efficiency map is reported (Figure 12). It can be clearly seen that for the lowest flow rate, the plateau is reached, saturating the heat transfer capability of the heat exchanger. As the hot fluid flow rate is increased, the effectiveness changes it shape, showing the maximum to be reached for low flow rate of the cold flow.

Table 3: Summary of experimental pressure losses, heat transfer, and heat exchanger effectiveness

T_hot (°C)	m_hot (kg/s)	m_cold (kg/s)	ΔP_hot (Pa)	ΔP_cold (Pa)	Q [W]	Effect. [%]
40.00	0.02	0.02	3179.2	0.00	174.0	64
200	0.1	0.1	40270	4238.9	8574	49

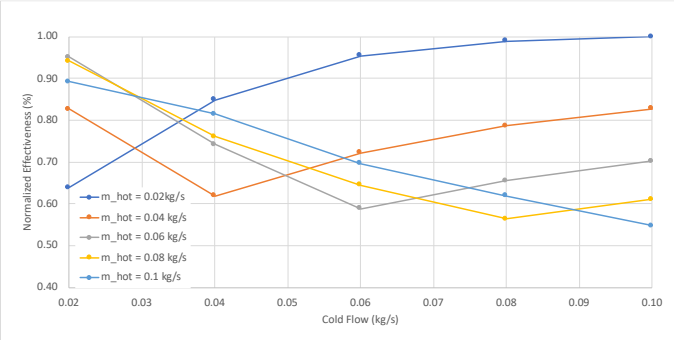

Figure 12: Normalized effectiveness of the heat exchanger. Hot fluid inlet temperature 200 °

7. NUMERICAL RESULTS

The ROM described in Section 3.3 is used to calculate the performance of the HX and the results are compared with the experimental tests in Table 4. Direct comparisons can be made on the heat duty and the pressure losses as these data are easily obtainable from the measurements, whilst other detailed performance will be described later. The computational model in case 1 (low flow rate, low temperature) returns a heat duty of 158 W and a pressure loss of 20 Pa on the hot fluid side and 4 Pa on the air side. The case 2 – high flow rate and high temperature – returns a heat duty of 11 081 W and pressure losses of 280 Pa and 40 Pa for the two sides. The heat flux discrepancy with respect to the experiments is negligible in case 1, while a discrepancy of about 2.5 kW is recorded on the high flow rate case. To further investigate the root cause of this not negligible discrepancy (about 30 % higher heat transfer in the high Re case, with order of magnitude differences in pressure losses in both cases), some in-depth considerations need to be made.

Table 4: Summary of ROM pressure losses and heat transfer estimates.

T_hot (°C)	m_hot (kg/s)	m_cold (kg/s)	ΔP_hot (Pa)	ΔP_cold (Pa)	Q [W]
40.00	0.02	0.02	158	4	158
200	0.1	0.1	280	40	11081

First, the experimental device is not insulated, and it is exposed to the lab environment. Therefore, natural convection plays an important role, as the temperature difference in the case 2 is about 170 ˚C. Using the actual surface area and a value of 10 W/m^2K as heat transfer coefficient for natural convection, it is reasonable to expect about 1 kW to heat to be dissipated into the environment (corresponding to the 10-12% discrepancy between the measured heat transfer on the hot and cold sides of the heat exchanger described in Section 6). Another heat transfer mechanism that is not considered in this work is the heat conduction via the inlet and outlet channel and via the supports of the HX. This effect is difficult to be quantified, but it will contribute in decreasing the actual heat transfer between fluids in the real application if compared to the theoretical value

Additional factors which may play an important role are the border effect (i.e. the regions where the flow is not periodic), which is neglected here, assuming identical behavior for all the cells, that might have a considerably different heat transfer.

Another important factor is the thermocouple placement. By having a single probe for the temperature measurement at the outlets, the measurement can be affected by a non-negligible uncertainty, as this probe assumes constant properties across the cross section, however the properties would vary across the channel cross-section, so it would be more accurate to have multiple probes and take an average.

The formulation of the ROM enables to have insight into the temperature evolution inside each HX layer. Figure 13 reports the temperature distribution for case 1. The cold flow proceeds in positive Y direction (bottom right to top left), while the hot flow is flowing left to right (positive X direction). The top surface refers to the temperature distribution of the hot flow, the lower one is referring to the cold flow. In Fig. 13, the temperature pattern shows a clear area in which the HX capability is saturated (bottom right corner and top left), where the two surfaces are very close to each other. In this area very little heat is transferred: indeed, the amount of heat transferred is proportional to the distance between the two surfaces along the z-axis as this represents the temperature difference across the membrane.

Figure 14 reports the other extreme case, where the temperature difference is very large among the two fluids. It is clear from Figure 12 that in this case the HT capabilities of the HX are exploited at the fullest, showing large heat transfer in all the regions of the HX. In this case, the efficiency is expected to be not as high as in the former case.

The discrepancies in the pressure losses between experiment and simulation are much more significant than the heat transfer, showing differences of orders of magnitude. Such a large step difference in this measurement is usually due to failures in turbulence and transition modelling in the simulation. The deficiencies of the RANS models used for the simulations in the present study have already been discussed in Section 4. Furthermore, the CFD simulations assumed very low turbulence intensity at the computational domain's inlet, and the transition to turbulence and eventual turbulence intensity will be very strongly dependent on this assumption. Additionally, the CFD simulations assumed a perfectly smooth wall. AM processes generally give high wall roughness, further increasing the turbulence intensity in the flow. During the experiment, the turbulence intensity and flow quality of the incoming flow to the

heat exchanger was not measured. It is likely that if the incoming flow was sufficiently turbulent the experimental pressure losses would be much higher than the values predicted by CFD.

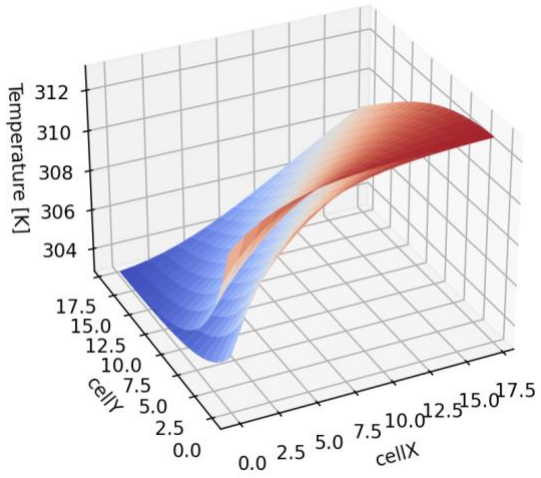

Figure 10: Performance for lowest flow rate and lowest temperature difference

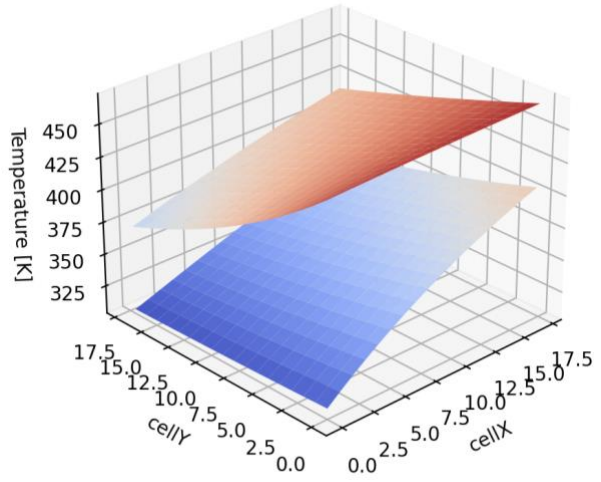

Figure 11: Performance for Highest flow rate and highest temperature difference

8. CONCLUSIONS AND NEXT STEPS

This work describes the design of a modular HX with physics based generative design tool as well as the development of a ROM to predict full scale heat exchanger performance. The designed heat exchanger was manufactured using a Laser-Powder Bed Fusion additive manufacturing process and experimentally tested. The goal of the work was to assess the capability of generative design tools to develop next-generation HXs for the aviation industry. The HX obtained by this method is a 20x20x20 array of a repeated unit cell. The unit cell is optimized for the design flow rate, showing high performance in terms of both increased heat transfer and reduced pressure losses.

With the demonstrated approach, HXs designed using physics-informed generative DfAM approaches are become a promising reality which could soon be adopted for the aviation industry. Indeed, the performance targets and weight target (not discussed here for confidentiality) are closely matched, and the repeating units is expected to eventually enable rapid certification of the entire catalogue of HXs based on the same unit cells.

The ROM based upon electrical analogy for heat transfer was validated for predictions of heat transfer, however predictions of the pressure drop across the heat exchanger were poor. Further development in the ROM will include the addition of:

- Border effects: as mentioned the inlet and outlet row of unit cells have different behavior with respect to the inner units, and this has an impact on heat transfer and pressure losses prediction.
- Heat dispersed to the environment: the outermost layers of unit cells might exchange heat with the environment due to natural convection. This aspect is not included in the current modeling and, as has been shown, may have a major impact.
- Better turbulence modelling.
- Feedback from manufacturing: the mismatch in pressure losses is likely due to real-geometry discrepancy from the CAD. This difference can be corrected by careful inspection and feedback from the actual geometry or CAD compensation techniques.

From this work a pragmatic way of using generative design technology is demonstrated that can greatly enhance the performance of heat exchangers. Software like ToffeeX enables designers equipped to improve state-of-the-art HXs without having a deep understanding of the TO methodology, making the designer available to focus on fluid-dynamics and thermal aspects rather than the mathematics. The capability of designing the unit cell for the specific flow rate and heat transfer requirement of each application makes it possible to have bespoke optimized solutions.

ACKNOWLEDGEMENTS

The authors would like to thank Abdul Haque and the AMRC for their assistance in manufacturing the heat exchanger.

REFERENCES

[1] A. S. Van Heerden, D. M. Judt, C. P. Lawson, T. Nikolaidis and D. Bosak, "Aircraft thermal management: Practices, technology, system architectures, future challenges, and opportunities," *Progress in Aerosapce Sciences,* vol. 128, 2022.

[2] K. E. Hinderliter, "Aircraft Thermal Management System". USA Patent 2017/0217592A1, 2017.

[3] F. Careri, R. H. U. Khan, C. Todd and M. M. Attalah, "Additive manufacturing of heat exchangers in aerospace applications: a review," *Applied Thermal Engineering,* vol. 235, 2023.

[4] H. Huang, L. J. Spadiccini and D. R. Sobel, "Fuel-cooled thermal management for advanced aeroengines," *J. Eng. Gas Turbines Power,* vol. 126, no. 2, pp. 284-293, 2004.

[5] B. P. Tucker, J. Homitz and J. Messmer, "System Integration of a thermal storage device for high-power-density systems," *SAE Technical Paper,* Vols. 2012-01-2189, 2012.

[6] G. Gvozdich, P. Weise and M. Von Spakovsky, "INVENT: Study of the Issues Involved in Integrating a Directed Energy Weapons Subsystem into a High Performance Aircraft System," in *50th AIAA Aerospace Sciences Meeting*, Nashville, TN, 2012.

[7] M. Williams, A. Muley, J. Bolla and H. Strumpf, "Advanced Heat Exchanger Technology for Aerospace Applications," *SAE Technical Paper,* Vols. 2008-01-2903, 2008.

[8] A. Muley, M. Stoia, D. Van Affelen, V. Reddy, V. Duggirala and S. Locke, "Recent Advances in Thin-Wall Additively Manufactured Heat Exchangers," in *ASME International Mechanical Engineering Congress and Exposition*, Virtual, 2021.

[9] I. Wadso and S. Holmqvist, Additively Manufactured Heat Exchangers, Thesis: Lund University, 2020.

[10] B. Blakey-Milner, P. Gradl, G. Snedden, M. Brooks, J. Pitot, E. Lopez, M. Leary, F. Berto and A. Du Plessis, "Metal additive manufacturing in aerospace: A review," *Materials and Design,* vol. 209, 2021.

[11] M. P. Bendsoe and O. Sigmund, Topology optimization: theory, methods, and applications, Springer Science \& Business Media, 2003.

[12] M. Pietropaoli, F. Montomoli and A. Gaymann, "Three-dimensional fluid topology optimization for heat transfer," *Structural and Multidisciplinary Optimization,* vol. 59, no. 1, pp. 801-812, 2019.

[13] K. Svanberg, "The method of moving asymptotes—a new method for structural optimization," *International journal for numerical methods in engineering,* vol. 24, no. 2, pp. 359-373, 1987.

[14] A. L. R. Prathyusha and G. Raghu Babu, "A review on additive manufacturing and topology optimization process for weight reduction studies in various industrial applications," *Materials Today: Proceedings,* vol. 62, no. 1, pp. 109-117, 2022.

[15] J. Alexandersen and C. S. Andreasen, "A review of topology optimisation for fluid-based problems," *Fluids,* vol. 29, no. 1, p. 29, 2020.

[16] P. Bettini, P. Alotto, V. Cirimele, R. Torchi and F. Lucchini, "Topology Optimization for Electromagnetics: A Survey," *IEEE Access,* vol. 10, no. 1, pp. 98593-98611, 2022.

[17] L. C. Høghøj, D. R. Nørhave, J. Alexandersen, O. Sigmund and C. S. Andreasen, "Topology optimization of two fluid heat exchangers," *International Journal of Heat and Mass Transfer,* vol. 163, no. 1, 2020.

[18] H. Kobayashi, K. Yaji, S. Yamasaki and K. Fujita, "Topology design of two-fluid heat exchanger," *Structural and Multidisciplinary Optimization,* vol. 63, no. 2, pp. 821-834, 2021.

[19] C. Lundgaard, J. Alexandersen, M. Zhou, C. S. Andreasen and O. Sigmund, "Revisiting density-based topology optimization for fluid-structure-interaction problems," *Structural and Multidisciplinary Optimization,* vol. 58, no. 1, pp. 969-995, 2018.